Springer

KSME

Journal of Mechanical Science and Technology 33 (11) (2019) 5243~5250
www.springerlink.com/content/1738-494x(Print)/1976-3824(Online)
DOI 10.1007/s12206-019-1014-6

Degradation and reduction of small punch creep life of service-exposed Super304H steel †

Thi Giang Le[1], Kee Bong Yoon[2,*] and Tae Min Jeong[1]

[1]*Graduate School, Department of Mechanical Engineering, Chung-Ang University, Seoul 06974, Korea*
[2]*Department of Mechanical Engineering, Chung-Ang University, Seoul 06974, Korea*

(Manuscript Received June 17, 2019; Revised August 28, 2019; Accepted August 28, 2019)

Abstract

To ensure the safety and structural integrity of a power boiler in thermal power plants, residual life management of superheater tubes at elevated temperature is needed. Over the decades, small punch (SP) creep testing has been widely used as an effective method for measuring creep life and creep properties of the boiler tube materials. In this study, a series of SP creep tests were performed at 650 °C with virgin and service-exposed Super304H stainless steels. The service period was 54750 h and 68550 h, respectively. The residual creep rupture life of the 68550 h serviced Super304H material decreased significantly when it was compared with the virgin and 54750 h serviced materials. Coarsening of the $M_{23}C_6$ precipitates along the grain boundaries made the adjacent region Cr-depleted, which could accelerate the formation of creep cavities at the grain boundaries. These microstructural degradations reduced the creep rupture life of the service-exposed materials. The Larson–Miller curve and the Monkman–Grant relationship were applied to predict the creep rupture life of service-exposed Super304H steels from the measured short creep rupture data.

Keywords: Super304H; Small punch creep; Creep life; Precipitate; Degradation; Superheater tube

1. Introduction

Super304H steel is an improved version of 18 %Cr–8 %Ni austenitic steel containing Cu, Nb, and N, which effectively increases its creep strength [1-3]. Because of its excellent creep and corrosion resistance at high temperatures, Super304H steel is increasingly used for the major components in power plants, aero-engines, and process plants operating at elevated temperatures of 550–750 °C [2-4]. It has been reported that the high-temperature creep strength of Super304H steel is due to finely dispersed precipitations, such as the Cu-rich precipitate, Nb(C,N) or $M_{23}C_6$ [3, 5]. However, long-term exposure of Super304H steel to high temperature must invite microstructural degradation and make the creep deformation plausible. This leads to the unexpected failure of the components, resulting in financial loss, environmental damage, and injuries [6, 7]. Therefore, it is vital to understand the material deterioration with time, assess the service damage of the components, and predict the residual life [7]. For assessing the residual life and the mechanical properties of Super304H steel at high temperature, either of the nondestructive testing methods or the direct creep life measuring methods with the conventional or miniature specimens, are commonly used [8]. Nondestructive testing method is employed to assess the residual life of the in-service components without introducing physical damage due to specimen sampling. However, accuracy in predicted life by the traditional nondestructive methods was often criticized. On the other hand, the direct creep life measuring technique usually provides reliable and accurate assessment results. But, for obtaining specimens of sufficient size, damage to the components is inevitable [8]. Hence, the small punch (SP) test was developed for estimating the mechanical properties of materials with miniature specimens [9]. The advantage of the SP test is that it is nearly nondestructive and does not cause any serious sampling damage [10, 11].

The SP creep test is considered effective for determining the creep properties of various types of materials at high temperatures, particularly between 550 and 750 °C [12-14]. Most studies verified that the SP creep test can reliably measure the creep properties of materials as well as the creep life [15]. The equivalence of the SP creep test to the standard uniaxial creep test was claimed based on the finite element simulations comparing the parameters obtained with the SP creep test with those obtained with the tensile creep test [16].

For the 304-type stainless steels, the SP creep test was successively applied for measuring the residual creep life of a service-exposed SA-304L material [11]. It was also used to

*Corresponding author. Tel.: +82 2 8205328, Fax.: +82 2 8126474
E-mail address: kbyoon@cau.ac.kr
† Recommended by Editor Chongdu Cho

Table 1. Standard chemical composition of Super304H steel (wt.%).

Material	C	Mn	P	S	Si	Cr	Ni	N	Nb	Al	B	Cu	Fe
ASTM A213M	0.07~ 0.13	Max 1.00	Max 0.040	Max 0.010	Max 0.30	17.0~ 19.0	7.5~ 10.5	0.05~ 0.12	0.30~ 0.60	0.003~ 0.030	0.001~ 0.010	2.50~ 3.50	Bal.

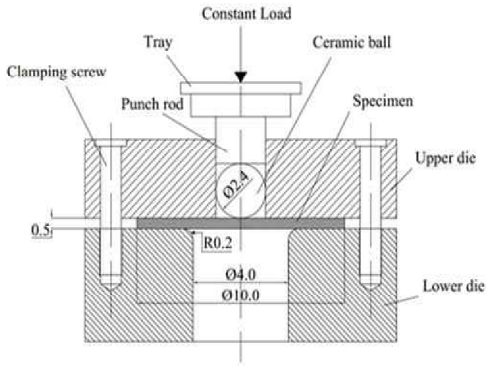

Fig. 1. Schematic of the SP creep testing jig.

optimize the N content in the range of 0.07–0.14 % of 316LN stainless steel for increasing the creep life [17]. These studies supported the advantage of the SP creep test method for the evaluation of the creep properties of the 304-type stainless steels. However, similar studies with the service-exposed Super304H stainless steel have not been reported yet.

The purpose of this study was to investigate the reduction of small punch creep life of service-exposed Super304H steel and degradation of microstructure causing the life reduction. The creep rupture life and creep deformation of the Super304H steels using a series of SP creep test at 650 °C under different loads were evaluated for virgin and service-exposed Super304H steels. The Larson–Miller parameter (LMP) and the Monkman–Grant relationship were used for prediction models. The effect of microstructural degradation due to long-term service exposure on the creep rupture life was discussed.

2. Experimental procedures

The material used in this study, Super304H steel, was taken from the serviced superheater boiler tubes of three different aging conditions, such as virgin and two service-exposed conditions at 596–650 °C for 54750 and 68550 hours. During service operation, the internal pressure of the superheater tubes was 4.8 MPa. The standard composition of this steel is shown in Table 1 [18].

Fig. 1 shows a cross-sectional schematic drawing of the SP creep test jig. It is composed of lower die, upper die, punch rod, small punch ball, and the specimen. The specimen was clamped between the lower die and the upper die. Constant load was applied to the center of the specimen using a ceramic ball with a diameter of 2.4 mm. The test specimen has a dimension of 10 mm × 10 mm × 0.5 mm. Before testing, the specimen was ground with SiC paper and then both sides were polished to minimize the surface roughness and obtain a thickness of 0.5 ± 0.002 mm. To avoid oxidation on the surface of the specimen during high temperature testing, Ar gas was provided into the furnace at a constant flow rate during the testing. The central deflection of the specimen was monitored by measuring the punch displacement versus time using a linear variable differential transformer with 1-μm resolution. The specimens for metallographic examination were prepared by polishing and were etched with the aqua regia solution containing HNO_3 and HCl (volume ratio of 1:3) for approximately 30 s.

In this study, a total of 12 SP creep test specimens were used for the virgin, 54750 h serviced, and 68550 h serviced Super304H steels. All the SP creep tests were performed at a temperature of 650 °C, with applied loads in the range of 400 to 500 N. The composition of the precipitates was analyzed using energy dispersive X-ray spectroscopy (EDS) together with scanning electron microscopy (SEM). The width of the Cr-depleted zones at the grain boundary was analyzed using field-emission scanning electron microscopy (FE-SEM) and EDS line scans.

The average size of the precipitates was determined using the ImageJ software (National Institutes of Health, USA) after binarization of each image into black and white [19-21]. A 125 μm × 95 μm area in the SEM images was analyzed to acquire statistics for the average size of the precipitates for the virgin and serviced materials. X-ray diffraction (XRD) was used to study the crystallinity of the specimens. Phase analysis was conducted with Cu Kα radiation ($\lambda = 0.1541$ nm) in the 2θ range from 40 to 80°.

3. Results and discussion

3.1 Microstructural degradation due to long-term service operation

Fig. 2 shows the XRD profiles of the virgin and 54750, and 68550 h serviced materials. The XRD results indicated the presence of Nb(C, N) and the γ-phase for all specimens. The presence of $M_{23}C_6$ phase was only found in the service-exposed materials. The lattice parameters of the γ phase were 0.3598 and 0.3591 nm for the virgin and two service-exposed materials, respectively. The main reason for the variation of the lattice parameter of the γ-phase was the solid solution of elements such as C, N, and Nb dissolved in the γ matrix. During the service time, specific elements of C, N, and Nb precipitated from the γ matrix and these formed Nb(C, N). Also $M_{23}C_6$ phase was formed and the lattice parameter for the γ matrix was decreased during the service. These two types of precipitates, Nb(C, N) and $M_{23}C_6$, were verified by SEM images (Figs. 3(a)-(c)) and EDS analyses (Figs. 3(d)

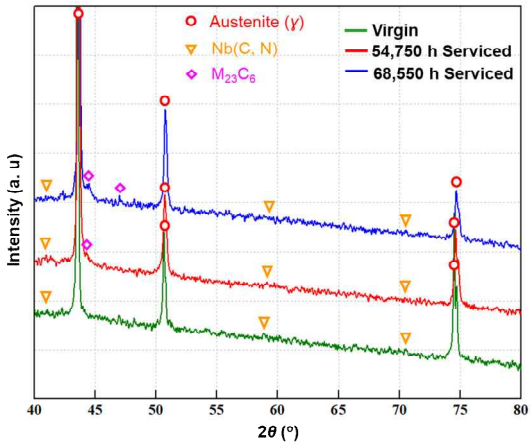

Fig. 2. XRD patterns for virgin and 54750 h, and 68550 h serviced materials.

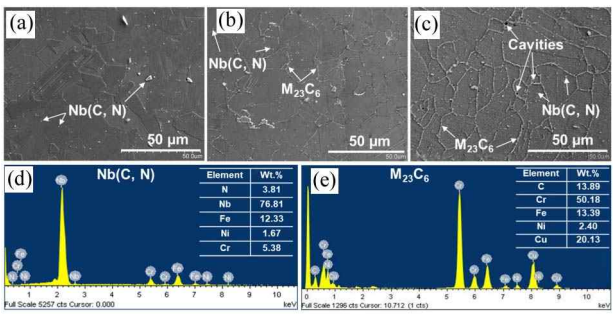

Fig. 3. SEM images of Super304H steel prior to the creep test: (a) Virgin; (b) 54750; (c) 68550 h serviced materials; EDS analysis for (d) Nb(C, N) precipitates; (e) $M_{23}C_6$ precipitates.

and (e)).

The Nb(C, N) precipitates were very fine with mainly the Nb element (76.81 wt.%) and its lattice parameter was 0.4441 nm and was stable during the service period. The lattice stabilities of the Nb(C, N) precipitates were based on the fact that the Gibbs energy of a compound depends on its composition at a given temperature [21]. This result agrees well with the stability of the size of the Nb(C, N) precipitates (Figs. 3(a)-(c)). These precipitates were observed in the austenitic grains and also at the grain boundaries. The $M_{23}C_6$ precipitates (M = Fe and Cr) shown in Figs. 3(b), (c) and (e) were observed along the grain boundaries in the serviced materials. Makarevicius et al. [22] found that the lattice parameter of $M_{23}C_6$ increased during the aging period. As aging progressed, Fe atoms in the precipitate lattice were partly substituted by Cr. Consequently, Cr atoms dominated in the $M_{23}C_6$ lattice [23]. Growth of $M_{23}C_6$ became more visible as aging time, and its granular shape changed gradually from fine to coarse shape. Simultaneously, the Cr-depleted zone was formed at the interface between the $M_{23}C_6$ precipitate and austenite. In previous studies [24], the Cr-depleted zone was presumed to be a sensitized boundary which could be a potential site for forming crack nucleation in the austenitic stainless steels. To show the Cr-

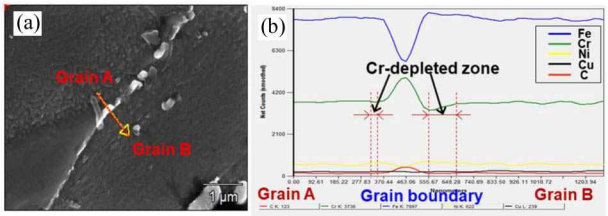

Fig. 4. (a) FE-SEM image; (b) X-ray line scan of elements across the grain boundary of 54750 h serviced Super304H steel.

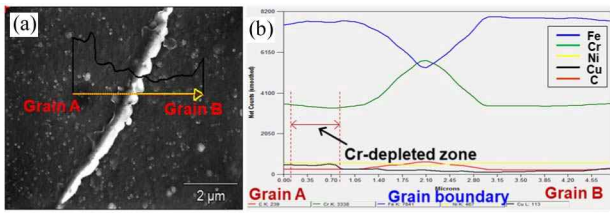

Fig. 5. (a) FE-SEM image; (b) X-ray line scan of elements across the grain boundary of 68550 h serviced Super304H steel.

depleted characteristics, FE-SEM images of net-count scans over the arrow line from grain A to grain B are shown in Figs. 4(a) and 5(a) for two aged specimens. The line scan was performed to determine the width of the Cr-depleted zone in the vicinity of the $M_{23}C_6$ precipitate. The width of the asymmetric Cr-depleted zone was estimated as about 100 nm (Fig. 4(b)) to ~700 nm (Fig. 5(b)) length as the service time increased from 54750 to 68550 h. If $M_{23}C_6$ precipitates formed more in the serviced Super304H steel materials, the Cr-depleted zone was formed more. According to the time-temperature-sensitization curve, Cr depletion at the grain boundaries can be started after 100 h at 650 °C [25]. Reduction of the creep life could be attributed to the increase in the size of the $M_{23}C_6$ precipitates [26]. In addition to these $M_{23}C_6$ precipitates, the Super304H steel could also have fine Cu-rich precipitates. It was shown by high-resolution transmission electron microscopy (TEM), since the resolution of SEM was not sufficient for detecting the finest Cu-rich precipitate even after very long-term service [27]. However, the peaks of the Cu-rich phase were difficult to record using XRD analysis because of their overlapping with the γ-phase. The extent of the coarsening depended on the Cu concentration in the alloy, as well as the duration and temperature of service [5].

In addition to the effect of the formation of the Cr-depleted zone in the microstructural degradation during service, the relations between the coarsening level of the precipitates and the service time were estimated. The average size of the precipitates was measured for the virgin and serviced materials. And, morphological characteristics of the precipitate were measured using the ImageJ software [28]. Fig. 6 shows images of the precipitates of the specimens, corresponding to the SEM images of Figs. 3(a)-(c) after ImageJ post-processing. The average sizes of the precipitates in the virgin and 54750, and 68550 h serviced materials were measured. The estimated average size of the precipitates was 0.563, 0.681, and

Table 2. SP creep test results for Super304H steel at 650 °C.

Service period (h)	Applied load (N)	Min. punch displacement rate (mm/h)	Rupture life (h)	LMP ($\times 10^3$)
Virgin	500	1.571E-02	26.9	19.780
	470	1.023E-02	38.3	19.921
	450	4.040E-03	68.0	20.151
	425	2.091E-03	280.0	20.719
54750	500	3.617E-02	15.9	19.569
	470	1.060E-02	27.3	19.786
	450	5.854E-03	52.9	20.051
	425	3.529E-03	75.2	20.192
68550	435	4.047E-02	10.4	19.399
	425	2.158E-02	19.9	19.659
	415	1.134E-02	41.2	19.951
	400	2.323E-03	212.8	20.609

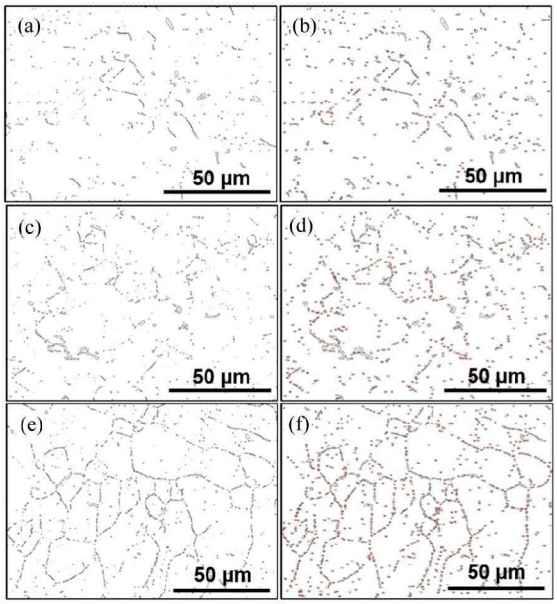

Fig. 6. Images of precipitates in the specimens, corresponding to Figs. 3(a)-(c) after image J post-processing, used for measuring the average size of precipitates: (a) and (b) Virgin; (c) and (d) 54750; (e) and (f) 68550 h serviced materials.

0.783 μm for the virgin and 54750, and 68550 h serviced materials, respectively. As the service time increased, the average size of the precipitates increased and material creep strength was significantly decreased.

3.2 SP creep properties

The SP creep test results are presented in Table 2 and Fig. 7. Fig. 7 shows the punch displacement versus time curves with various loads at 650 °C for the virgin, 54750, and 68550 h serviced materials. These punch displacement data were converted into punch-displacement rate data by using the seven-point incremental polynomial method of ASTM-E647. Fig. 8

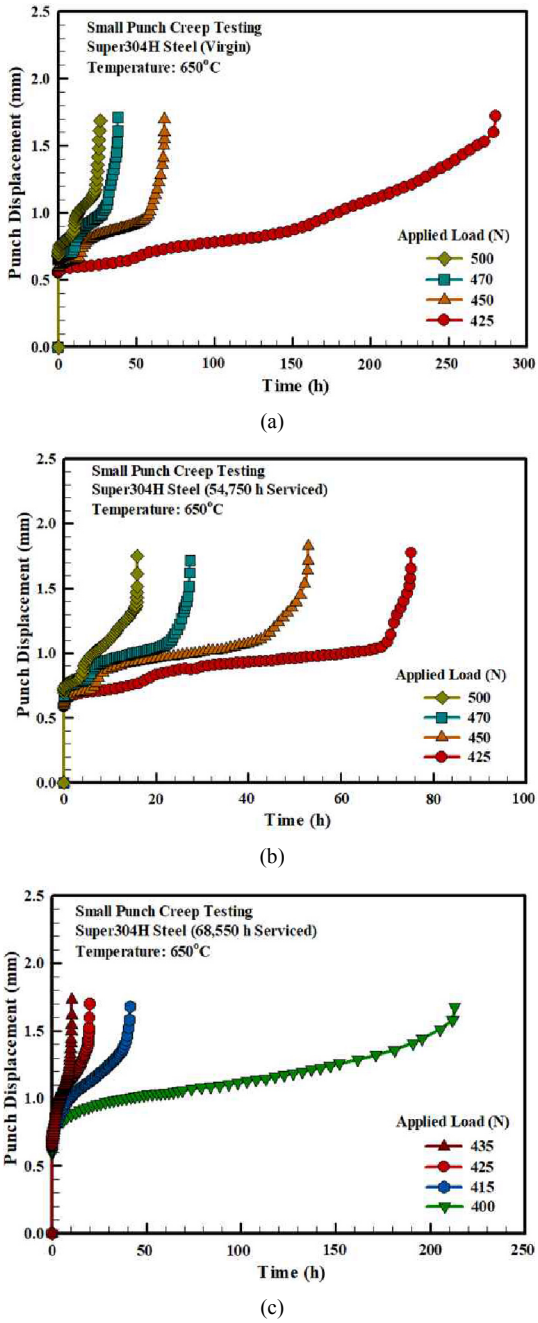

Fig. 7. SP creep displacement versus time for Super304H steel at 650 °C: (a) Virgin; (b) 54750 h serviced; (c) 68550 h serviced materials.

shows the curves converted into punch-displacement rate versus time curves in log–log scale. In all specimens, double minima were observed in the punch-displacement rate. The double minima are characteristics showing the early crack initiation of the SP specimens [12, 13]. The SP creep curves have various creep stages such as double primary, secondary, and tertiary stages. After load application, instantaneous deformation occurred caused by the bending deformation as the contact area between the ball and the upper surface of the specimen [29]. This instantaneous deformation was increased as the applied load increased from 400 to 500 N. The primary

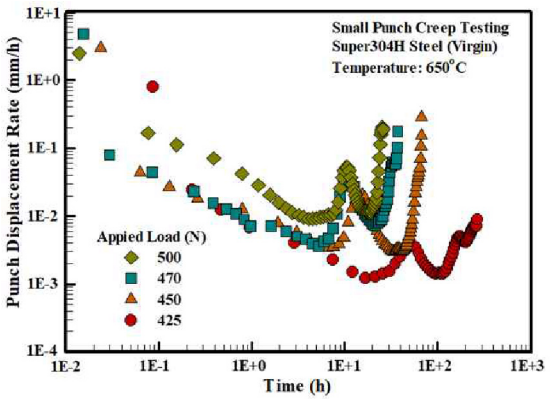

(a)

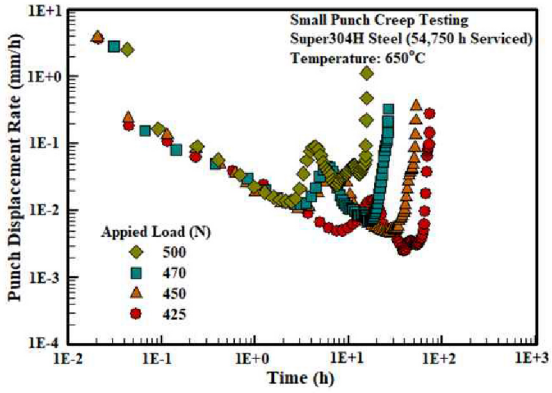

(b)

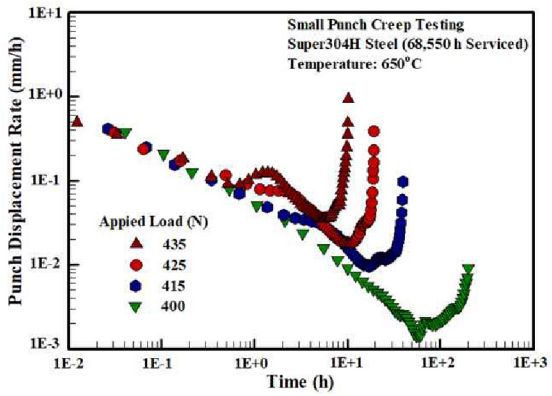

(c)

Fig. 8. SP displacement rate versus time for Super304H steel at 650 °C: (a) Virgin; (b) 54750 h serviced; (c) 68550 h serviced materials.

creep stage was characterized by a displacement rate decreasing over time. In the subsequent secondary creep stage, the displacement rate remained constant and reached a minimum value, determined as shown in Table 2. In the tertiary creep stage, the contact region between the ball and specimen increased with the increase in the displacement, accompanied by a significant thickness reduction, and localized necking led to deformation of the specimen. The crack development caused a rapid deformation progression and resulted in rupture. For the virgin and 54750 h serviced materials, the duration of the primary and tertiary creep stages of the graphs was too short compared with the rupture life, while the tertiary creep stage of the 68550 h serviced material appeared to start at approximately 40 % of the rupture life. This result could be explained by early formation of crack initiation at the cavities in the Cr-depleted zone, as indicated by the microstructural degradation observation results for the 68550 h serviced material prior to the SP creep test. Fig. 9 shows comparisons of the SP creep curves of the virgin, 54750 h and 68550 h serviced materials under the same applied load (425 N) at 650 °C. The creep rupture life of the 68550 h serviced material was considerably shorter than that of the other two materials. In Fig. 10, SEM photography of the fracture shapes of the SP creep specimens for the virgin and service-exposed materials were also compared. It was shown that several circumferential cracks were formed in all of the virgin and the service-exposed materials.

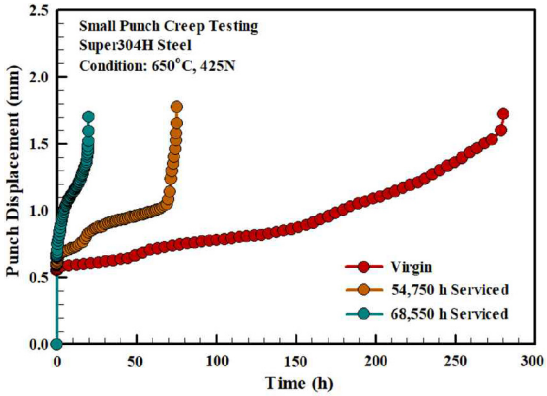

Fig. 9. Comparisons of the SP creep curves among virgin, 54750 h and 68550 h serviced Super304H steel under 425 N at 650 °C.

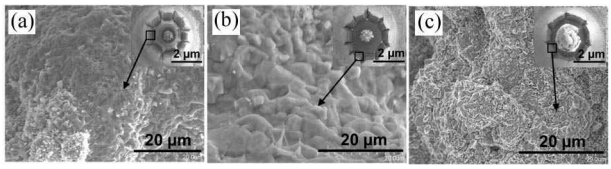

Fig. 10. Fracture shapes of the SP creep specimens for (a) virgin and service-exposed materials after; (b) 54750 h; (c) 68550 h under 425 N at 650 °C.

The relationship between the minimum punch displacement rate ($\dot{\delta}_{\min}$) and the applied load (P) in the SP creep test can be described by a power law in a similar manner to the well-known Norton's power law creep constitutive equation, as expressed in Eq. (1) [20]:

$$\dot{\delta}_{\min} = \bar{A}P^{\bar{n}} \tag{1}$$

where $\bar{A}$ and $\bar{n}$ are the SP creep coefficient and SP creep exponent, respectively.

A linear regression line (Fig. 11) was fitted to the data for the virgin and serviced materials, respectively. The results of regression lines and the values of $\bar{A}$ and $\bar{n}$ are shown in Table 3 and Fig. 11.

Table 3. Creep coefficient and creep exponent for Super304H steel according to Norton's power law for creep.

Material	$\bar{A}\left(N^{-\bar{n}}\cdot \mathrm{mm}\cdot \mathrm{h}^{-1}\right)$	$\bar{n}$
Virgin	1.62×10^{-37}	12.98
54750 h serviced	6.49×10^{-41}	14.33
68550 h serviced	9.79×10^{-92}	33.98

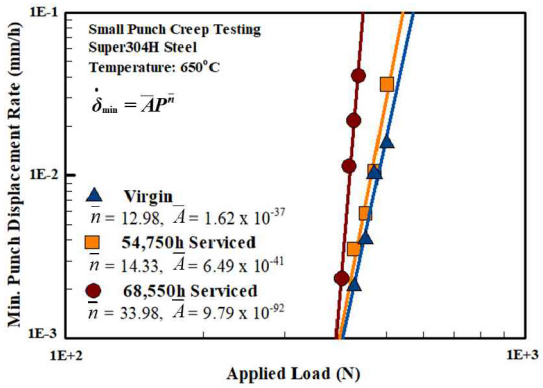

Fig. 11. Relationship between the minimum displacement rate and the applied SP load for Super304H steel at 650 °C.

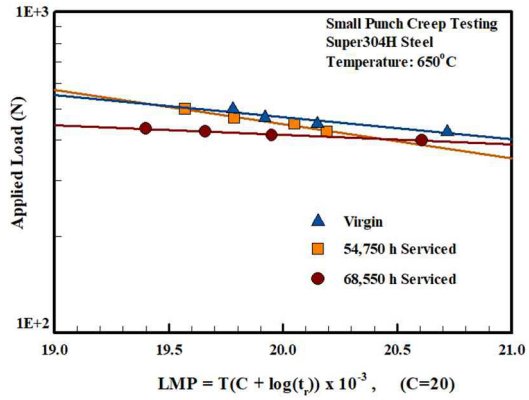

Fig. 12. Comparison of the rupture life data of Super304H steel at 650 °C: Applied load versus the LMP.

The SP creep exponent ($\bar{n}$) was determined by the slope of the regression line as 12.98, 14.33, and 33.98 for the virgin and 54750 h and 68550 h serviced materials, respectively. As shown in Fig. 11, the creep exponent values of the virgin and 54750 h serviced materials are very close, indicating that the two materials have similar creep behavior. However, the creep exponent of the 68550 h serviced material is significantly larger than that of the other two materials. If the minimum punch displacement rate is compared under a specific applied load of 425 N, Fig. 11 shows that the minimum punch displacement rate of the 68550 h serviced material was approximately ten-times and six-times larger than that of the virgin and 54750 h serviced materials, respectively. It indicates that the degradation of the 68550 h serviced material was much progressed compared with that of 54750 h serviced material.

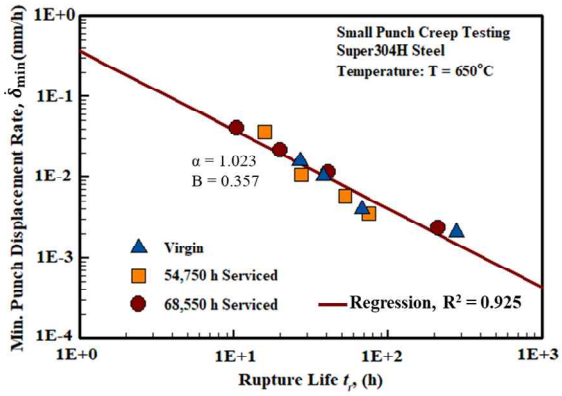

Fig. 13. Relationship between the minimum displacement rate and the rupture life for Super304H steel at 650 °C.

Since, the microstructural degradation of 68550 h serviced material such as coarsening of $M_{23}C_6$ precipitates and forming of cavities along the grain boundaries was quite significant compared with the other two materials. This argument is consistent with the observation shown in Figs. 3-5.

Using uniaxial creep tests, Bagui et al. [5] obtained creep exponents of 17 and 10.7 at 600 and 750 °C, respectively. Sahoo et al. [26] estimated the creep exponents of 304H steel to be 9.57, 7.76, and 7.46 at 650, 700, and 750 °C, respectively. These results show that the creep exponent decreases with an increase in the temperature, owing to thermally activated dislocation motion for the dislocation creep [26]. For comparing the uniaxial creep constants with the constants obtained from the SP creep test, the power law equation shown in Eq. (1) should be converted to Norton's power law creep equation by converting the SP applied load (N) to the equivalent uniaxial stress (MPa), and the SP punch displacement rate (mm/h) to the uniaxial creep strain rate (1/h).

To estimate the creep rupture life for the virgin and serviced materials, the LMP was calculated using Eq. (2).

$$LMP = T\left(C + \log\left(t_r\right)\right), \tag{2}$$

where T is the temperature (in Kelvin), C = 20 is the Larson–Miller constant, and t_r is the time to rupture (in hours). The calculated results for the LMP values are also included in Table 2. Fig. 12 shows the difference in SP creep rupture life between the virgin and serviced-exposed materials. The SP creep lives of the service-exposed specimens were shorter than the virgin material under the same applied load condition. The relationship between the applied load and the LMP value including the creep rupture life and operating temperature was established. Using this LMP model the creep rupture life of the service-exposed materials can be predicted.

The minimum punch displacement rate ($\dot{\delta}_{\min}$) and the rupture life (t_r) was expressed by the Monkman–Grant relationship as follows in Eq. (3) [13].

$$t_r\dot{\delta}_{\min}^{\alpha} = B\,. \tag{3}$$

Here, α is a constant close to unity, and B is the Monkman–Grant constant for SP creep testing. Similar to the uniaxial creep case of the Monkman–Grant relationship, a linear correlation was clearly observed in the SP creep case too as shown in Fig. 13. The Monkman–Grant relationship was followed by not only the virgin material but also the service-exposed materials. The confidence level for the regression line (R^2) was approximately 0.925. The values of α and B were determined to be 1.023 and 0.357, respectively. The minimum displacement rate correlated well with the SP rupture life, with a slope of approximately 0.978, which is close to the expected value for SUS304H with the addition of small amounts of V (~0.962) [13] and 304HCu (~0.975) [26]. The Monkman–Grant relationship can be used to predict the SP creep rupture life of serviced materials according to the minimum punch-displacement rate as supported by other investigation too [30].

4. Conclusions

SP creep testing was applied to evaluate the creep rupture life of Super304H steel with different service-exposed conditions of superheater boiler tubes taken from a domestic power plant. The following conclusions were obtained.

(1) The reductions in the creep rupture life of the service-exposed materials were different for different service conditions. The creep rupture behavior of the virgin and the 54750 h serviced materials showed similar characteristics, while the 68550 h serviced material showed considerably short creep life compared with those of the other materials.

(2) During the high temperature service period, material degradation of the Super304H steel could occur as follows. The main strengthening phase of Nb(C, N) precipitates did not change significantly in size. On the other hand, precipitation of the $M_{23}C_6$ progressively occurred and coarsening of the precipitate occurred quickly along the grain boundaries. This generated Cr-depleted zones near the precipitated grain boundaries. This could promote the formation of cavities and affect the material creep resistance.

(3) The LMP model was applied to predict the SP creep rupture life. The LMP curves were obtained from the test data conducted at four different load levels and at 650 °C for the virgin and the service-exposed materials. This LMP model can be used to predict the SP creep rupture life for this materials. It was also shown that the Monkman–Grant linear relationship of the SP creep data can provide an effective way to predict SP creep rupture life for this material.

Acknowledgments

This work was supported by a Korea Institute of Energy Technology Evaluation and Planning (KETEP) [grant number 2014 1010101850] funded by the Ministry of Trade, Industry and Energy (MOTIE). This study was also supported by a KETEP [grant number 2016 1110100090] funded by the MOTIE.

Nomenclature

$\bar{A}$	: Small punch creep coefficient
$\bar{n}$	: Small punch creep exponent
B	: Monkman–Grant constant
C	: Larson–Miller constant
LMP	: Larson–Miller parameter
P	: Small punch load
t_r	: Time to rupture (in hours)
T	: Temperature (in Kelvin)
$\dot{\delta}_{\min}$	: Minimum punch-displacement rate
α	: Monkman-Grant exponent for small punch creep

References

[1] F. Masuyama, History of power plants and progress in heat resistant steels, *ISIJ International*, 41 (6) (2001) 612-625.

[2] M. K. Dash, T. Karthikeyan, R. Mythili, V. D. Vijayanand and S. Saroja, Effect of long-term thermal exposures on microstructure and impression creep in 304HCu grade austenitic stainless steel, *Metallurgical and Materials Transactions A*, 48 (10) (2017) 4883-4894.

[3] D. B. Park, S. M. Hong, K. H. Lee, M. Y. Huh, J. Y. Suh, S. C. Lee and W. S. Jung, High-temperature creep behavior and microstructural evolution of an 18Cr9Ni3CuNbVN austenitic stainless steel, *Materials Characterization*, 93 (2014) 52-61.

[4] X. Huang, Q. Zhou, W. Wang, W. S. Li and Y. Gao, Microstructure and property evolutions of a novel Super304H steel during high temperature creeping, *Materials at High Temperatures*, 35 (5) (2017) 438-450.

[5] S. Bagui, K. Laha, R. Mitra and S. Tarafder, Accelerated creep behavior of Nb and Cu added 18Cr-8Ni austenitic stainless steel, *Materials Research Express*, 5 (11) (2018) 116515.

[6] H. Tanaka, M. Murata, F. Abe and H. Irie, Microstructural evolution and change in hardness in type 304H stainless steel during long-term creep, *Materials Science and Engineering A*, 319-321 (2001) 788-791.

[7] V. H. Dao, K. B. Yoon, G. M. Yang and J. S. Oh, Determination of creep constitutive model for 28-48WCo alloy based on experimental creep tests at 817-982 °C, *J. of Mechanical Science and Technology,* 32 (9) (2018) 4201-4208.

[8] S. Yang, J. Zhou, X. Ling and Z. Yang, Effect of geometric factors and processing parameters on plastic damage of SUS304 stainless steel by small punch test, *Materials and Design*, 41 (2012) 447-452.

[9] M. P. Manahan, A. S. Argon and O. K. Harling, The development of a miniaturized disk bend test for the determination of postirradiation mechanical properties, *J. of Nuclear Materials*, 104 (1981) 1545-1550.

[10] T. Izaki, T. Kobayashi, J. Kusumoto and A. Kanaya, A creep life assessment method for boiler pipes using small punch creep test, *International J. of Pressure Vessel Piping*, 86 (9) (2009) 637-642.

[11] A. Moradi, N. Soltani and H. Nobakhti, Experimental study of remaining creep life of SA-304L stainless steel using small punch creep test, *Materials at High Temperatures*, 35 (5) (2017) 410-417.
[12] N. C. Z. Htun, T. T. Nguyen, D. Won, M. H. Nguyen and K. B. Yoon, Creep fracture behaviour of SUS304H steel with vanadium addition based on small punch creep testing, *Materials at High Temperatures*, 34 (1) (2017) 33-40.
[13] N. C. Z. Htun, T. T. Nguyen, K. B. Yoon and J. H Park, Small punch and uniaxial creep fracture behaviours of modified SUS304H steel at various temperatures, *Materials at High Temperatures*, 35 (4) (2018) 378-386.
[14] S. I. Komazaki, T. Kato, Y. Kohno and H. Tanigawa, Creep property measurements of welded joint of reduced-activation ferritic steel by the small-punch creep test, *Materials Science and Engineering A*, 510-511 (C) (2009) 229-233.
[15] Y. W. Ma, S. Shim and K. B. Yoon, Assessment of power law creep constants of Gr91 steel using small punch creep tests, *Fatigue and Fracture Engineering Materials and Structures*, 32 (12) (2009) 951-960.
[16] M. D. Mathew, J. G. Kumar, V. Ganesan and K. Laha, Small punch creep studies for optimization of nitrogen content in 316LN SS for enhanced creep resistance, *Metallurgical and Materials Transactions A*, 45 (2) (2014) 731-737.
[17] F. D. Persio, G. C. Stratford and R. C. Hurst, Validation of the small punch test as a method for assessing ageing of a V modified low alloy steel, *Proc. of the Baltica VI International Conference on Life Management and Maintenance for Power Plants*, Helsinki, Finland, 2 (2004) 523-535.
[18] *ASTM A213/213M: Standard Specification for Steamless Ferritic and Austenitic Alloy-steel Boiler, Superheater, and Heat-exchanger Tubes*, ASTM International (2003).
[19] T. Zhou, R. P. Babu, J. Odqvist, H. Yu and P. Hedström, Quantitative electron microscopy and physically based modeling of Cu precipitation in precipitation-hardening martensitic stainless steel 15-5 PH, *Materials and Design*, 143 (2018) 141-149.
[20] Q. Xiong, J. D. Robson, L. Chang, J. W. Fellowes and M. C. Smith, Numerical simulation of grain boundary carbides evolution in 316H stainless steel, *J. of Nuclear Materials*, 508 (2018) 299-309.
[21] M. Hillert, The compound energy formalism, *Journal of Alloys and Compounds*, 320 (2) (2001) 161-176.
[22] V. Makarevičius, V. Baltušnikas, I. Lukošiūtė, R. Kriūkienė and A. Grybėnas, Transformation kinetic of $M_{23}C_6$ carbide lattice parameters in ferritic-martensitic P91 steel during thermal ageing, *Proc. of Metal*, Brno, Czech Republic (2015) 2-6.
[23] S. Yamasaki, Modelling precipitation of carbides in martensitic steels, *Doctoral Thesis*, University of Cambridge, UK (2004).
[24] S. R. Ortner, A stem study of the effect of precipitation on grain boundary chemistry in AISI 304 steel, *Acta Metallurgica et Materialia*, 39 (3) (1991) 341-350.
[25] X. M. Li, Y. Zou, Z. W. Zhang, Z. D. Zou and B. S. Du, Intergranular corrosion of weld metal of super type 304H steel during 650 °C aging, *Corrosion*, 68 (2012) 379-387.
[26] K. C. Sahoo, S. Goyal, V. Ganesan, J. Vanaja, G. V. Reddy, P. Padmanabhan and S. K. Laha, Analysis of creep deformation and damage behaviour of 304HCu austenitic stainless steel, *Materials at High Temperatures* (2019) 1-16.
[27] C. Y. Chi, H. Y. Yu, J. X. Dong, W. Q. Li, S. C. Cheng, Z. D. Liu and X. S. Xie, The precipitation strengthening behavior of Cu-rich phase in Nb contained advanced Fe-Cr-Ni type austenitic heat resistant steel for USC power plant application, *Progress in Natural Science: Materials International*, 23 (3) (2012) 175-185.
[28] Y. Li, Y. Yang, Y. Wu, L. Wang and X. Liu, Quantitative comparison of three Ni-containing phases to the elevated-temperature properties of Al-Si piston alloys, *Materials Science and Engineering A*, 527 (26) (2010) 7132-7137.
[29] S. Yang, X. Ling and Y. Zheng, Creep behaviors evaluation of Incoloy800H by small punch creep test, *Materials Science and Engineering A,* 685 (2017) 1-6.
[30] A. O. Mariscal, M. L. S. Munoz, Naveena and S. Komazaki, Application of small punch creep testing for evaluation of creep properties of as-received, *Materials Science and Engineering A*, 709 (2018) 322-329.

Thi Giang Le received her B.S. in Metallurgical Engineering from Hanoi University of Science and Technology. She received the M.S. in Mechanical Engineering from Chung-Ang University. She is currently a Ph.D. candidate at Chung-Ang University. Her research interest is creep behavior and aging characteristics of high temperature alloy materials.

Kee Bong Yoon received his M.S. in Mechanical Engineering from KAIST and Ph.D. from Georgia Institute of Technology. He is currently a Professor at Chung-Ang University. His research interests are high temperature fracture and risk based management of energy plants. He is extending research to fracture of additive manufactured materials.

Tae Min Jeong received his B.S. and M.S. in Mechanical Engineering from Chung-Ang University. He conducted research on creep behavior and fracture of the high temperature materials. He is also interested in the life and integrity assessment of plant facilities. He is currently working on the team of NAND package front technology of SK Hynix Inc.